Applied Thermal Engineering 159 (2019) 113982

Contents lists available at ScienceDirect

Applied Thermal Engineering

journal homepage: www.elsevier.com/locate/apthermeng

Research Paper

Experimental investigation of a miniature loop heat pipe with eccentric evaporator for cooling electronics

Wei Tian, Song He, Zhichun Liu*, Wei Liu

School of Energy and Power Engineering, Huazhong University of Science and Technology, 430074 Wuhan, China

HIGHLIGHTS

- An mLHP with 4.5 mm thick eccentric ELR was proposed and fabricated.
- The proposed mLHP can manage a wide range of heat loads from 2 W to 60 W.
- Impact of sink temperature on the mLHP operation was tested and analyzed.

ARTICLE INFO

Keywords:
Loop heat pipe
Flat evaporator
Longitudinal replenishment
Eccentric structure
Electronics cooling

ABSTRACT

In the study, a miniature loop heat pipe (mLHP) that employed a flat disk type evaporator with longitudinal replenishment was presented. The biporous wick was fabricated from sintered nickel powders and was eccentrically installed in the cavity of the evaporator to simultaneously form the evaporation and compensation section. Methanol was selected as the working fluid with a charge ratio of 80%. The total length of the mLHP system corresponded to 750 mm. In the study, the temperature of the heat sink was varied from 0 °C to 35 °C. The experimental results demonstrated that the proposed mLHP starts up successfully under a heat load ranging from 2 W to 60 W in the horizontal orientation. Additionally, the mLHP system exhibited a good response to a low heat load. The thermal resistance of the evaporator and LHP decreased with increases in the heat load, and a minimum R_{evap} of 0.27 °C/W was obtained at a heat load of 60 W. The effect of different heat sink temperatures on the performance of the mLHP was analyzed in the study.

1. Introduction

Given the application of integrated circuits and Microelectromechanical Systems (MEMS), there are significant developments in the electronics industry in recent years. Electronic equipment with high performance and small size are increasingly popular, and thus the thermal management of high flux electronic equipment constitutes a significant challenge. Loop heat pipes (LHPs) are highly effective heat transfer devices that utilize the phase-change latent heat to transfer heat with capillary force from the wick to drive the working fluid, and the LHPs are considered as a viable thermal control solution to improve the operating performance of electronics. When compared with conventional heat pipes, LHPs offer a few advantages such as separated phase-change parts and long-distance heat transfer [1,2]. Since the 1970s, several extant studies have focused on operating characteristics and performance improvement in LHPs for the successful application of LHP systems to electronic device cooling [3–7].

With respect to mobile electronics, such as mobile phones and laptop, there are more demanding requirements including high power density, response to low heat load, and limited space. In a manner different from evaporators with opposite replenishment (EOR), evaporators with longitudinal replenishment (ELR) are thinner [8]. The thickness of ELR is reduced to 3–8 mm, and the value is typically in the range of 10 to 20 mm for EOR. Therefore, numerous innovative designs based on ELR were proposed in recent years [9,10]. Li et al. [11] presented a miniature loop heat pipe (mLHP) with a 1.2-mm thick flat evaporator. The mLHP employed a sintered copper mesh wick in the evaporator and liquid line to obtain a stronger capillary force. The mLHP was tested under air convection at 24 °C and was successfully operated at a low heat load of 2 W in the horizontal orientation. The minimum thermal resistance of the system was 0.111 °C/W at a heat load of 11 W in a gravity favorable mode. Wang et al. [12,13] developed a copper-water mLHP with an 8-mm thick flat rectangular evaporator. The mLHP operated at the high heat load of 110 W.

* Corresponding author.
E-mail address: zcliu@hust.edu.cn (Z. Liu).

https://doi.org/10.1016/j.applthermaleng.2019.113982
Received 26 December 2018; Received in revised form 3 June 2019; Accepted 16 June 2019
Available online 17 June 2019
1359-4311/

Nomenclature

Cp	specific heat at constant pressure, J/(kg·°C)
G	thermal conductance, W/°C
h	latent heat, kJ/kg
P	pressure, Pa
Q	heat load, W
R	thermal resistance, °C/W
T	temperature, °C
β	charging ratio
$\dot{m}$	mass flux, kg/s

Subscripts

a	ambiance
cc	compensation chamber
cc-if	the liquid in the compensation chamber
cc-wall	compensation chamber wall
cond	condenser
cond-in	condenser inlet
cond-out	condenser outlet
evap	evaporator
evap-if	saturated vapor in the evaporator
evap-in	evaporator inlet
evap-out	evaporator outlet
evap-wall	evaporator wall
g	gravity
groove	vapor removal groove
heat	heat source
l	liquid
ll	liquid line
sink	heat sink
sys	system
tot	total
v	vapor
vl	vapor line
w	wall
wick	wick

Additionally, the temperature oscillation during start-up and the effect of different condenser locations and operating orientations were tested, and thereby confirmed that the condenser located close to the evaporator outlet positively affected the operating performance of mLHP with ELR. Shioga et al. [14] demonstrated a micro loop heat pipe (μLHP) that was designed to fit the casing of a smartphone with a thickness of 0.6 mm for an evaporator without the compensation chamber. The μLHP was manufactured from six layers of copper plates with a thickness of 0.1 mm that were formed via chemical etching on the copper. A minimum LHP thermal resistance corresponding to 0.32 °C/W was obtained at a maximal heat load of 15 W. The μLHP exhibited a good response to the periodic power input. Singh et al. [15,16] improved an mLHP by changing the position of the compensation chamber. When compared with the disk shape design, the thickness of the evaporator with rectangular shape design decreased from 10 mm to 5 mm. The mLHP disposed of the maximum heat load of 70 W with the minimum total thermal resistance corresponding to 1.5 °C/W. Tang et al. [17] developed a new approach that combines the ploughing-extrusion method with a chemical method to fabricate a micro V-grooves aluminum wick. The wick with new structure could be observed excellent hydrophilicity and capillary performance in the capillary height rise tests. Similarly, Esarte et al. [18] designed and built the wick with the 3D selective laser melting printing technique (SLM). The geometry and pore size could be controlled according to different demands. It is important to improve the performance of the LHP system performance. Maydanik et al. [19,20] investigated a copper miniature loop heat pipe equipped with a flat evaporator that measured 80 × 42 × 7 mm. The mLHP was experimentally evaluated with different working fluids. With water as the working fluid, the mLHP transferred the maximum heat load corresponding to 1200 W at a vapor temperature of 103.4 °C. Additionally, the influence of different orientations in the gravity field and heat sink temperatures was tested when acetone was used as the working fluid. The mLHP was successfully operated at heat loads ranging from 5 W to 60 W with heat sink temperatures ranging from −40 °C to +50 °C. It should be noted that the operation mode of mLHP changed from variable conductivity to constant conductivity across the complete range of heat loads. Lee et al. [21] devised a thin planar bifacial evaporator with a bifacial wick structure to use the advantages offered by evaporators with longitudinal replenishment that exhibit the possibility of delivering the heat load on the two sides. Steady-state and transient state response performances of the mLHP were examined in detail, and the relationship between fluid inventories and operational characteristics was discussed.

There is a paucity of extant studies that focus on ELRs in contrast to that focus on EORs. However, it is viewed as a potential solution to electronic device cooling given the numerous important results obtained in previous studies. A disadvantage of limiting ELRs applications is that its ability to provide liquid to the evaporation interface is worse than that of the EORs. The contact area between the compensation chamber and wick in the ELRs is smaller than that in the EORs. Additionally, it is necessary to transport the working fluid farther in ELRs. Given this disadvantage, the range of heat loads at which the LHP can operate is significantly reduced. High-performance CPUs used in mobile electronics require a better response to low loads and also higher full-load power. For example, the 8th Generation Intel® Core™ i9 Processors exhibit a thermal design power corresponding to 45 W and a packing size is corresponding to 42 × 28 mm. Therefore, it is extremely challenging in terms of LHP.

The main objective of the present study included the development and investigation of a new type of mLHP with a flat evaporator with longitudinal replenishment to improve the performance at low heat loads and increase the range of heat loads for the mLHP application. An mLHP was presented with eccentric evaporator structure. The thickness of the evaporator corresponded to 4.5 mm with a biporous wick composed of sintered nickel powder. The startup performance and operation characteristics of the mLHP were tested and analyzed at varying heat sink temperatures and heat loads.

2. Experimental setup

The structure of the miniature LHP system is shown in Fig. 1. The mLHP consisted of the following four components: a flat evaporator, vapor line, liquid line, and condenser with a concentric pipe structure. The height of the flat evaporator was 4.5 mm, and the thickness of the wall of the evaporator was 0.5 mm. An eccentric design was adopted to increase the contact area between the compensation chamber and wick. As shown in Fig. 1(b) and (c), the compensation chamber is on the same plane as the wick, and the eccentric structure of the porous wick increases the volume of the compensation chamber. The wick with 3.5-mm thickness corresponded to a biporous structure that was sintered with nickel powder and Na_2CO_3. There were seven vapor grooves in the wick to collect the vapor. The vapor line, liquid line, and condenser were formed of copper tubing with an initial internal/external diameter of 3/4 mm, 4/6 mm, and 4/6 mm, respectively. The condenser line was cooled via a constant temperature water jacket. The total length of the mLHP system was 745 mm and was comparable to that of traditional

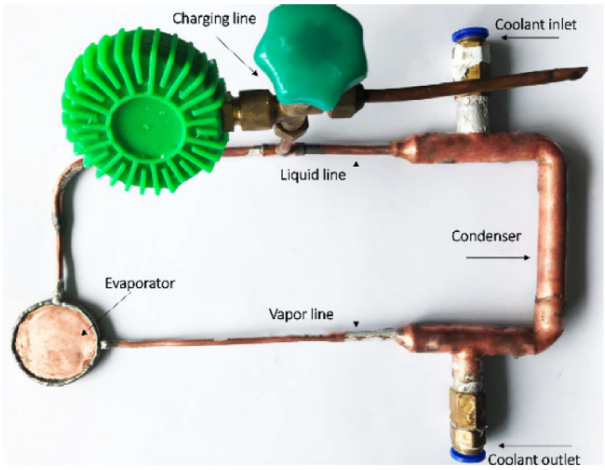

(a) mLHP prototype

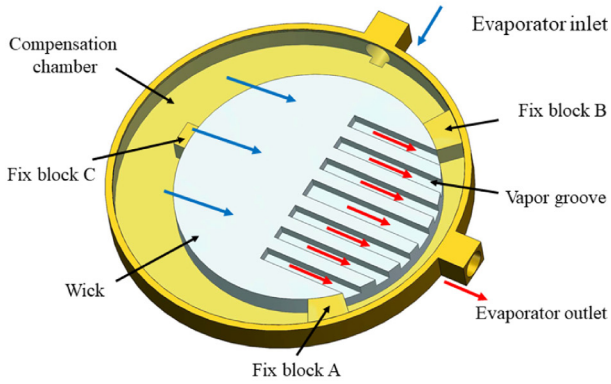

(b) Structure of the evaporator

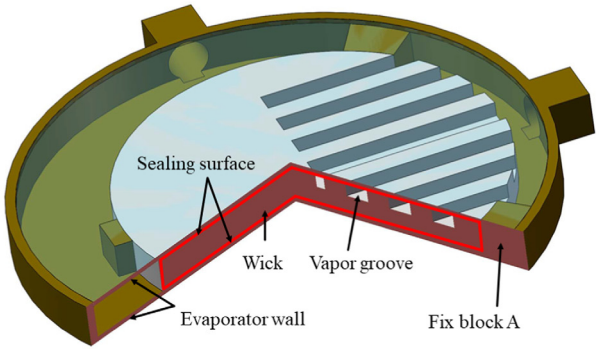

(c) section view of the evaporator

Fig. 1. mLHP experimental prototype.

LHP systems. In the study, methanol with a purity of 99.5% was selected as the working fluid. Prior to when the liquid is charged into the mLHP, the system is vacuumed to a negative pressure state when the pressure is 2.4×10^{-4} Pa to reduce the negative effects of non-condensable gases. A charging ratio β corresponding to 80% is selected and calculated as follows:

$$\beta = \frac{V_{charge}}{V_{tot}} \times 100\% \quad (1)$$

where V_{charge} denotes the volume of the working fluid and V_{tot} denotes the total volume of the inner space of the mLHP. Table 1 lists the geometric and material characteristics of the experimental mLHP.

The mLHP test system is shown in Fig. 2. The experimental system comprises of the following four parts: heating system, data acquisition system, cooling water recirculation system, and an mLHP. A 30-mm diameter cylinder with three embedded heaters (which are controlled via a voltage regulator and wattmeter) simulates the heating module to provide power input. A double pipe condenser connected with a thermostatic circulating water sink is used to cool the vapor within the condenser. The temperature of the thermostatic circulating water sink during the tests ranges from 0 to 35 °C. The ambient temperature in the laboratory room is maintained at 25 °C (± 2 °C). In order to avoid the heat loss of the system to the environment, the loop is wrapped in insulated cotton, and the cylinder block surface is covered with a 10-mm thick nano-adiabatic material wherein the thermal conductivity is 0.012 W/(m·K). The temperature is measured via T-type thermocouples with an accuracy of ± 0.5 °C. A Keithley-2700 data acquisition system connected with thermocouples is used to monitor and record the test data from the LHP at a time interval of 1 s. To avoid the effect of gravity on the experimental results, the mLHP was operated in the horizontal orientation during the experiment. Additionally, the startup performance and operation characteristics of the mLHP is tested and analyzed at varying heat sink temperatures and heat loads.

3. Experimental and results

3.1. Characteristic of the startup process

The startup is the most important and complicated process for an mLHP operation, and it is typically viewed as an extremely effective indicator for LHP thermal performance. Generally, a successful startup is defined as that when the temperature of the LHP reaches the steady state from the initial state after the heat load is applied. However, the results also indicate that the startup phenomena of an LHP are classified into several modes based on different characteristics of startup performance as follows: (1) oscillating mode, (2) overshoot startup, and (3) stable startup [22]. The temperature of the evaporator increases immediately when a heat load is applied to the LHP. The working fluid absorbs the heat and evaporates. When sufficient pressure difference is produced across the wick, the working fluid vapor flows out from the evaporator to the condenser and returns to the compensation chamber when the liquid phase flows through the vapor grooves, vapor line, and liquid line. Based on the operating principle of the LHP, the working fluid is driven to cycle via the capillary force due to the evaporation of liquid in the porous wick. It should be equal to or exceed the total loop pressure drop due to the circling of the working fluid. When pressure is balanced, the temperature of the LHP is stable, and the startup ends. The total loop pressure drop is expressed as follows:

Table 1
Geometric parameters of the mLHP.

Components	Dimensions	Value
Evaporator	OD/height (mm)	50/4.5
	Material	brass
Wick	OD/height (mm)	38/3.5
	Porosity	71%
	material	nickel
Vapor groove	Width × height (mm)	2 × 1.5
Vapor line	ID/OD (mm)	3/4
	Length (mm)	175
Liquid line	ID/OD (mm)	4/6
	Length (mm)	255
Condenser	ID/OD (mm)	4/6
	Length (mm)	320
Heat block	Dimensions (mm)	30
Working fluid		methanol
Charging ratio		80%
mLHP	Total length (mm)	750

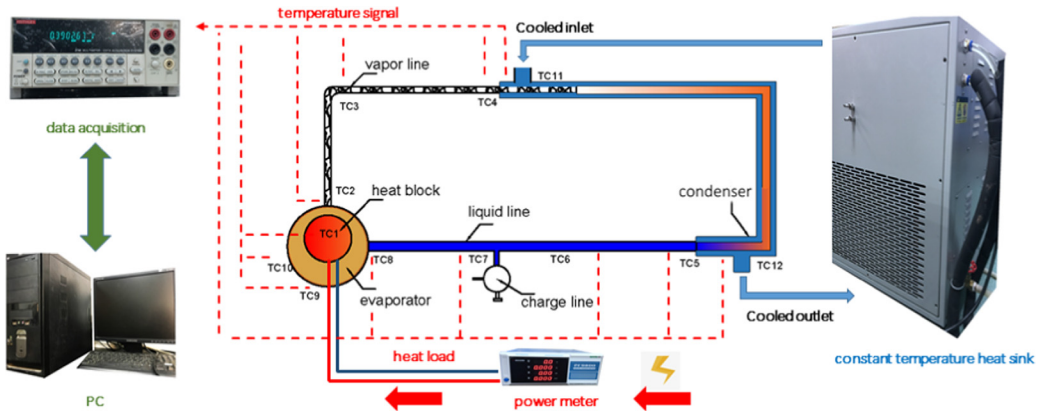

TC1: temperature of the heat source, T_{heat}; TC2: temperature of the evaporator outlet,$T_{evap\text{-}out}$; TC3: temperature of the vapor line,T_{vv}; TC4: temperature of the condenser inlet, $T_{cond\text{-}in}$; TC5: temperature of the condenser outlet ,$T_{cond\text{-}out}$; TC6, TC7: temperature of the liquid line, T_{ll}; TC8: temperature of the evaporator inlet , $T_{evap\text{-}in}$; TC9, TC10: temperature of the evaporator wall, $T_{evap\text{-}wall}$

Fig. 2. Schematic of the mLHP experimental system.

$$\Delta P_{tot} = \Delta P_{grovve} + \Delta P_{vl} + \Delta P_{cond} + \Delta P_{ll} + \Delta P_{wick} + \Delta P_g \quad (2)$$

where the terms on the right-hand side denote the pressure drops in the groove, vapor line, condenser, liquid line, wick, and gravity, respectively [23,24].

Based on extant studies, there is a minimum heat load for a particular LHP system to start successfully. Decreases in the value could increase the range of heat load that the LHP can operate in. Therefore, the mLHP requires lower values if it is applied to mobile electronic devices. In the present study, the mLHP is tested at a heat load ranging from 2 W to 60 W to investigate the characteristics of the startup process. The temperature range of the heat sink is set from 0 °C to 35 °C. All tests were performed in a horizontal orientation.

Generally, the operation performance of the ELRs is affected by the size and structure of the compensation chamber. The volume and area connected with the wick of the compensation chamber in ELRs are significantly smaller than those in the EORs as shown in Fig. 3. Decreases in the compensation chamber and liquid absorption area make it increasingly difficult to supply the liquid. Furthermore, as shown in Fig. 3, the liquid flowing path from absorption surface (in compensation chamber) to evaporation surface in ELRs is longer and increasingly complicated when compared with that in the EORs, and thus the thermal performance of the ELRs is lower than that of the EORs. Simultaneously, the compensation chamber and the evaporator share a heated surface. The structure of the evaporator leads to more significant heat leaks through the side. As shown in Fig. 1(b), when compared with the existing design of mLHP, the present eccentric structure provides a larger compensation chamber and liquid supplying area for the porous wick and obtains a better balance involving smaller thickness, better response to the low heat load, and greater heat load range.

Fig. 4 shows the temperature of the mLHP during the startup process with the sink temperature set of 10 °C. As shown in Fig. 4(a), the mLHP starts successfully and operates stably at the heat load of 2 W in the horizontal orientation when T_{heat} corresponds to 29.3 °C. When the heat load is applied to the mLHP, $T_{evap\text{-}out}$ and $T_{evap\text{-}in}$ increase with increases in T_{heat}. Thus, $T_{cond\text{-}in}$ slowly increases. After approximately 15 min, $T_{cond\text{-}in}$ begins to increase rapidly and reaches a stable oscillation condition. Furthermore, T_{heat} is stable under 30 °C, and $T_{evap\text{-}out}$ periodically exhibits slight fluctuations with the oscillation of $T_{cond\text{-}out}$. It is observed that $T_{evap\text{-}out}$ and $T_{evap\text{-}in}$ are extremely close, and T_{ll} is significantly lower than $T_{evap\text{-}in}$. The operation of the mLHP is in a stable state. The startup process is divided into three stages. First, for stage I, T_{heat}, $T_{evap\text{-}out}$, and $T_{evap\text{-}in}$ rapidly increase as soon as the heat load is applied to the evaporator while the other temperatures of the mLHP increase slowly or remain in the initial state. The working fluid begins to cycle when temperature and pressure difference are obtained under a certain heat load. When the operation is in stage II, the working fluid is redistributed in the entire mLHP, and the vapor enters into the condenser through vapor line and begins to condensate after which the condensate liquid form of the fluid returns to the evaporator due to the action of the pressure difference. Finally, the operation of the mLHP reaches a stable state wherein the pressure decrease due to the cycling of the working fluid and capillary force due to the heat load are balanced, i.e., stage III.

In a manner different from the low heat load of 2 W, the characteristic of the startup process at heat loads of 10 W and 60 W is shown in Fig. 4(b) and (c), respectively. In Fig. 4(b), with respect to the heat load of 10 W, T_{ll} increases with respect to $T_{evap\text{-}out}$ and $T_{evap\text{-}in}$ in stage I.

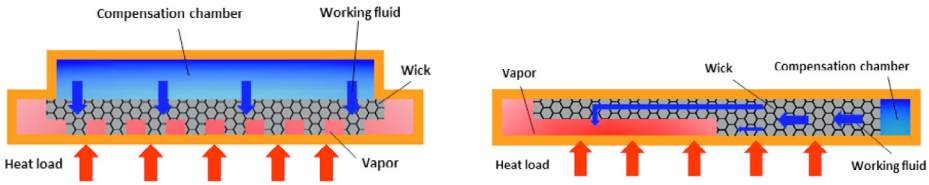

(a) Evaporator with opposite replenishment (b) Evaporator with longitudinal replenishment

Fig. 3. Scheme of the active zone of different types of flat evaporators.

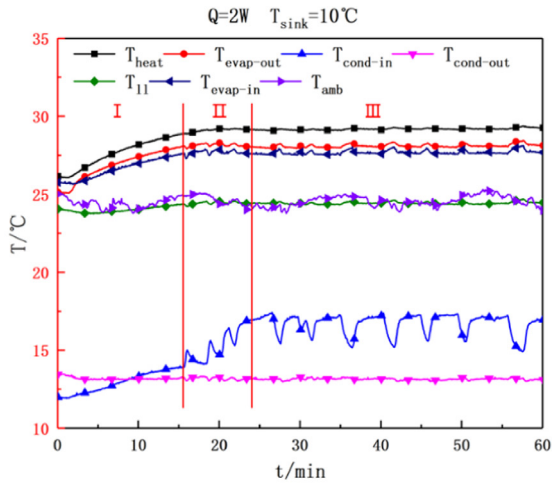

(a) Q=2 W T_{sink}=10 °C

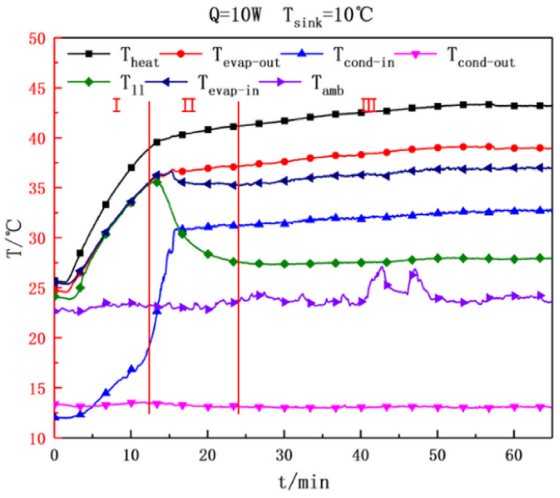

(b) Q=10 W T_{sink}=10 °C

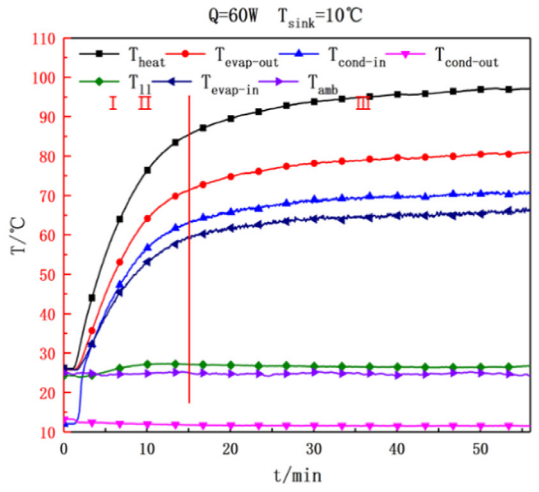

(c) Q=60 W T_{sink}=10 °C

Fig. 4. Startup process at T_{sink} = 10 °C.

After approximately 12 min, T_{ll} and $T_{evap\text{-}in}$ decrease simultaneously when $T_{cond\text{-}in}$ significantly increases. The phenomenon implies that the working fluid is cycled and the compensation chamber is cooled by the returning liquid form of the working fluid. A temperature difference

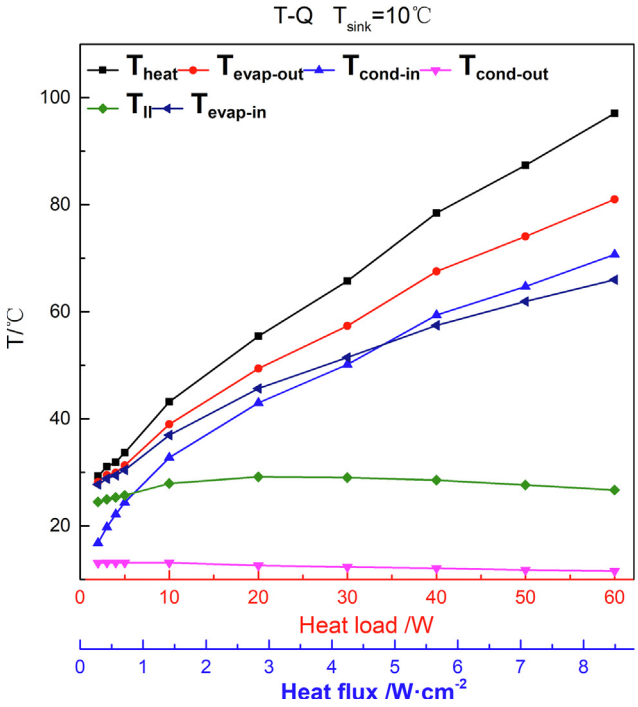

Fig. 5. Changes in temperature with different heat loads.

occurs between the outlet and inlet of the evaporator. However, as shown in Fig. 4(c), at the heat load of 60 W, $T_{cond\text{-}in}$ initially increases with increases in $T_{evap\text{-}out}$. There is no turning point at which $T_{cond\text{-}in}$ increases rapidly and T_{ll} decreases. The first and second stages are almost simultaneously performed. Additionally, the oscillation of $T_{cond\text{-}in}$ decreases when the heat load increases. This is because the location of the gas-liquid interface changes. The condensation vapor/liquid interface is located in the vapor line at a heat load of 2 W and in the condenser at a heat load of 60 W, respectively. Based on previous studies, it is generally recognized that, under the heat load limit for LHP, a high heat load is better for the startup process than a low heat load because the increase of the temperature difference between the evaporator and the compensation which results in the pressure difference between these two components becomes more instant. Thus, the first stage of the startup process is completed quickly under a high heat load. However, the third stage at the high heat load is longer. As shown in Fig. 4(c), it takes a long time to obtain a stable state at high heat load.

Fig. 5 shows the operation temperature with different heat loads at the sink temperature of 10 °C in a steady state. As shown in Fig. 5, the temperatures for the heating wall, evaporator outlet, condenser inlet, and evaporator inlet increase with increases in the heat load although the temperatures for liquid line and condenser outlet decrease with increases in the heat load. This is because the mass flux of the working fluid increases with increases in the heat load.

3.2. Effect of different heat sink temperatures

Fig. 6 shows the mLHP operation temperature of different parts under different heat load values Q (5 W, 20 W, 40 W, and 60 W) relative to different heat sink temperatures. It is observed that the stable operation temperature of the LHP increases with increases in the sink temperature. Furthermore, changes in the outlet temperature of the condenser are in tune with the sink temperature under different conditions, and this implies that the applied heat load is completely dissipated by the condenser.

In order to reveal the effect of different sink temperatures, a thermal network method is used to analyze the thermal characteristics of the evaporator and compensation chamber. Fig. 7 shows the thermal

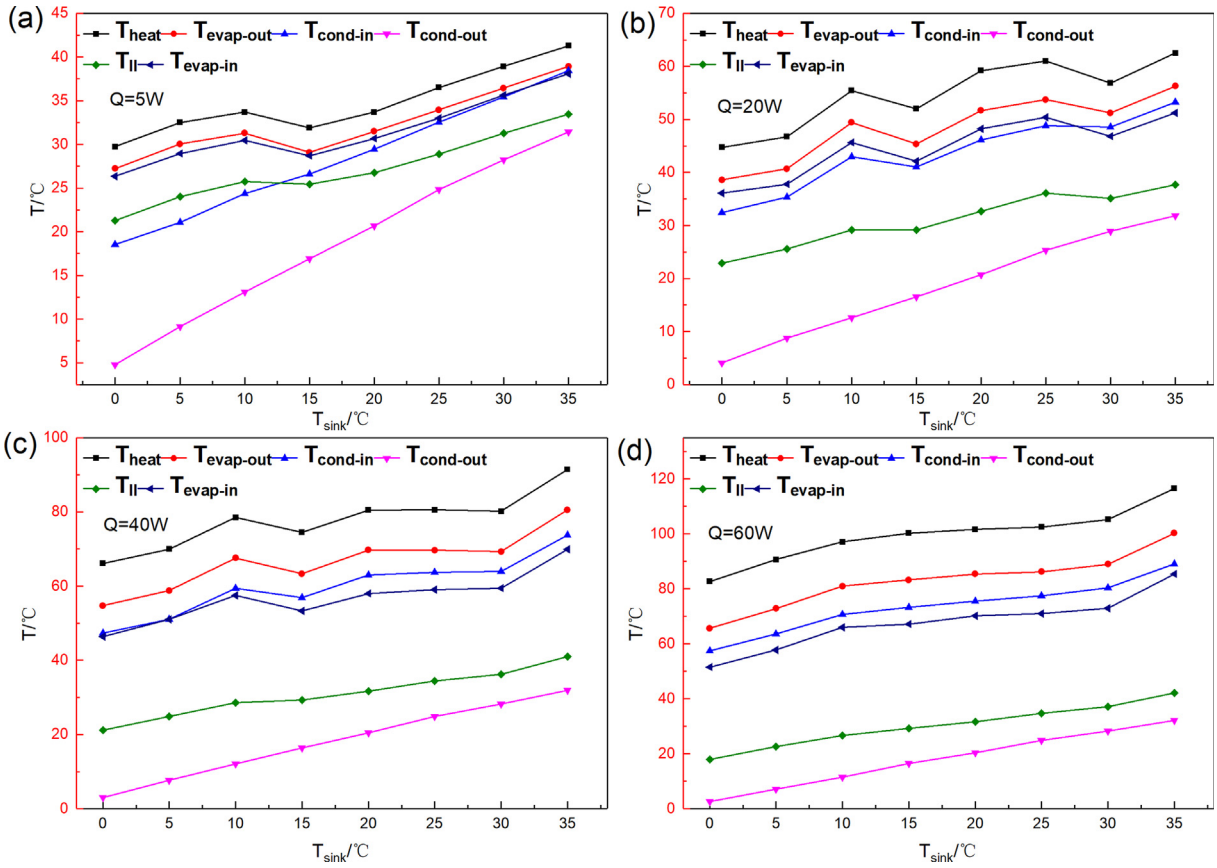

Fig. 6. mLHP operation temperature relative to different heat loads and different heat sink temperatures.

network for the evaporator and compensation chamber.

The heat load Q that is transferred from the heat source to the heat surface evaporator is divided into three parts. Most of the heat load $Q_{evap\text{-}wall,if}$ is transferred through the vapor channel to the wick. Part of the heat load $Q_{wall,evap\text{-}cc}$ is transferred through the wall of the evaporator to the compensation chamber. Only a small part of the heat load Q_R is absorbed by the vapor of the working fluid. It is assumed that the thermal conductance of different parts does not change at different sink temperatures in the stable state under a certain heat load Q. In order to transfer the same heat load, the temperature difference between different parts will be considered constant with different heat sink temperature. Therefore, the analysis of $Q_{if,evap\text{-}cc}$ is the key to determine the effect of different heat sink temperatures, which denotes the heat loads absorbed during the temperature of the working fluid liquid increase from $T_{evap\text{-}if}$ to $T_{cc\text{-}if}$. The temperature difference between $T_{evap\text{-}if}$ and $T_{cc\text{-}if}$ should be constant based on the law of conservation of energy. Therefore, $T_{evap\text{-}if}$ and the operation temperature of LHP will increase when $T_{evap\text{-}in}$ and $T_{cc\text{-}if}$ increase with increases in the temperature of the heat sink. The results of the previous analyses indicate that the effect of different sink temperature is mainly reflected in the temperature of reflux and the environment of the compensation chamber. The increases in the heat sink temperature worsen the environment of the compensation chamber and increase the operation temperature of the LHP.

The temperature changes of the mLHP and the liquid line at different sink temperature of 5 °C and 25 °C is shown in Figs. 8 and 9. T_{ll1} denotes the temperature of the liquid line point near the condenser. T_{ll2} denotes the temperature of the liquid line point near the evaporator. It

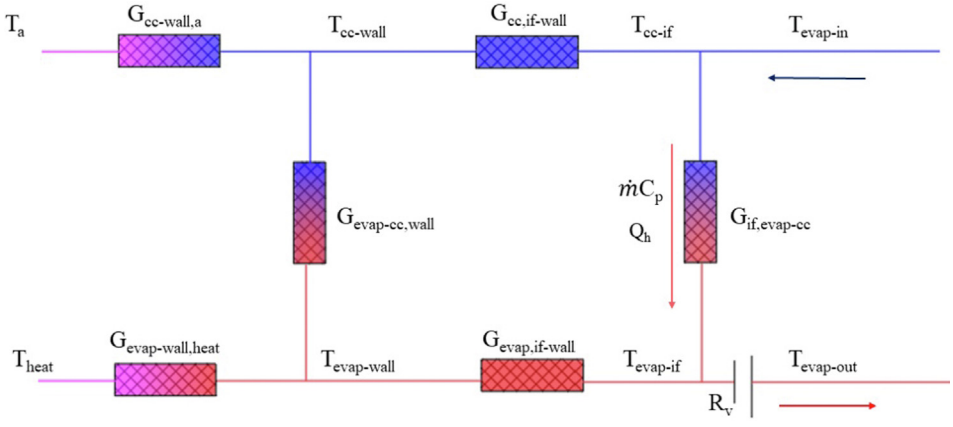

Fig. 7. Thermal network for the evaporator and compensation chamber.

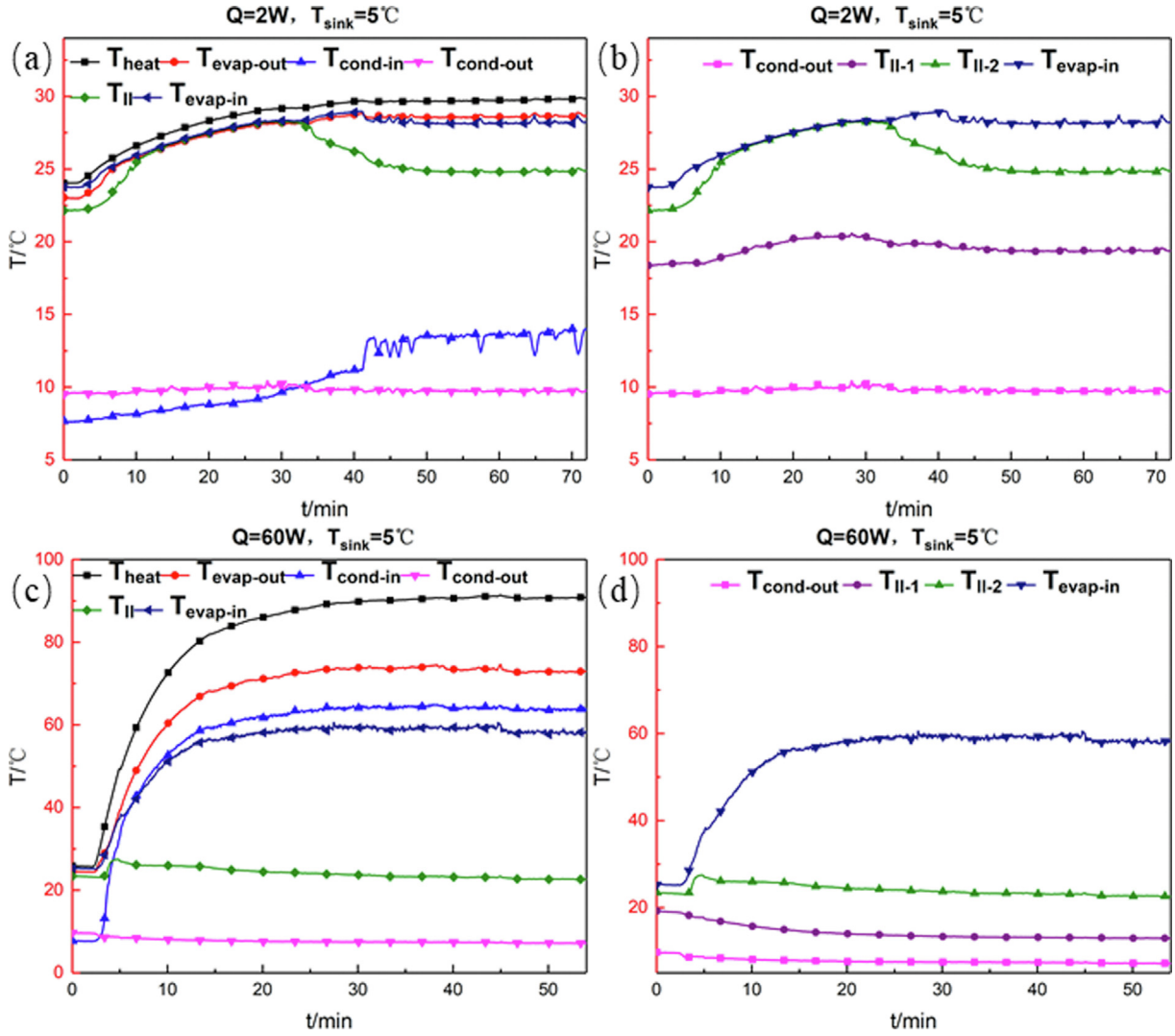

Fig. 8. The temperature of the mLHP at the sink temperature of 5 ˚C.

can be observed that there is a response sign to the heat load in the liquid line whether at high load or low load. The temperature of the liquid line begins to decrease from 30 min until the mLHP reaches a steady state at the heat load of 2 W. The time point is about 4 min at the heat load of 60 W. The decrease of the liquid temperature means that the start-up process of the mLHP enters the stage II. Meanwhile, there is a significant temperature gradient in the liquid line due to the transfer of heat from the compensation chamber to the condenser. Under certain conditions, such as the sink temperature of 25 ˚C and the heat load of 60 W, the stage II will be transient and insignificant on account of the combined effect of heat from the condenser and the compensating chamber.

3.3. Thermal resistance

Thermal resistance is another important parameter to evaluate the thermal performance of LHP to transfer heat from electronics. Specifically, R_{LHP} denotes the total thermal resistance of LHP in the experiment. The evaporating thermal resistance R_{evap} is used to reflect the performance of the porous wick in the evaporator. The system thermal resistance Rsys is used to show the heat transfer performance of the overall system in the experiment [25]. The R_{LHP}, $R_{evap,}$ and R_{sys} are typically defined by the following equations:

$$R_{heat} = \frac{T_{heat} - T_e}{Q} \tag{3}$$

$$R_{LHP} = \frac{T_e - T_c}{Q} \tag{4}$$

$$R_{sys} = \frac{T_{heat} - T_{sink}}{Q} \tag{5}$$

where T_e denotes the average of evaporator temperature (TC1 + TC2)/2, T_{cond} denotes the average of condenser temperature, T_{sink} denotes the heat sink temperature, and Q denotes the input heat load.

Generally, the thermal resistance varies between constant thermal resistance state and varying thermal resistance state with changes in the heat load. Fig. 10 shows the thermal resistance dependence of heat load and sink temperature in the tests. At the same sink temperature of 10 ˚C, the R_{evap}, $R_{LHP,}$ and R_{sys} decrease with increases in the heat load. Additionally, R_{evap} changes from 0.569 ˚C/W at the heat load of 2 W to 0.269 ˚C/W at the heat load of 60 W. The R_{LHP} is similar to R_{evap} that changes from 6.890 ˚C/W to 0.799 ˚C /W and the R_{sys} changes from 9.365 ˚C/W to 1.317 ˚C/W. The change in thermal resistance exhibits the same trend wherein it decreases with increases in the thermal load at the total test range of the sink temperature. This implies that the thermal resistance changes from a varying thermal resistance state to a constant thermal resistance state.

The change in thermal resistance is mainly caused by the change of

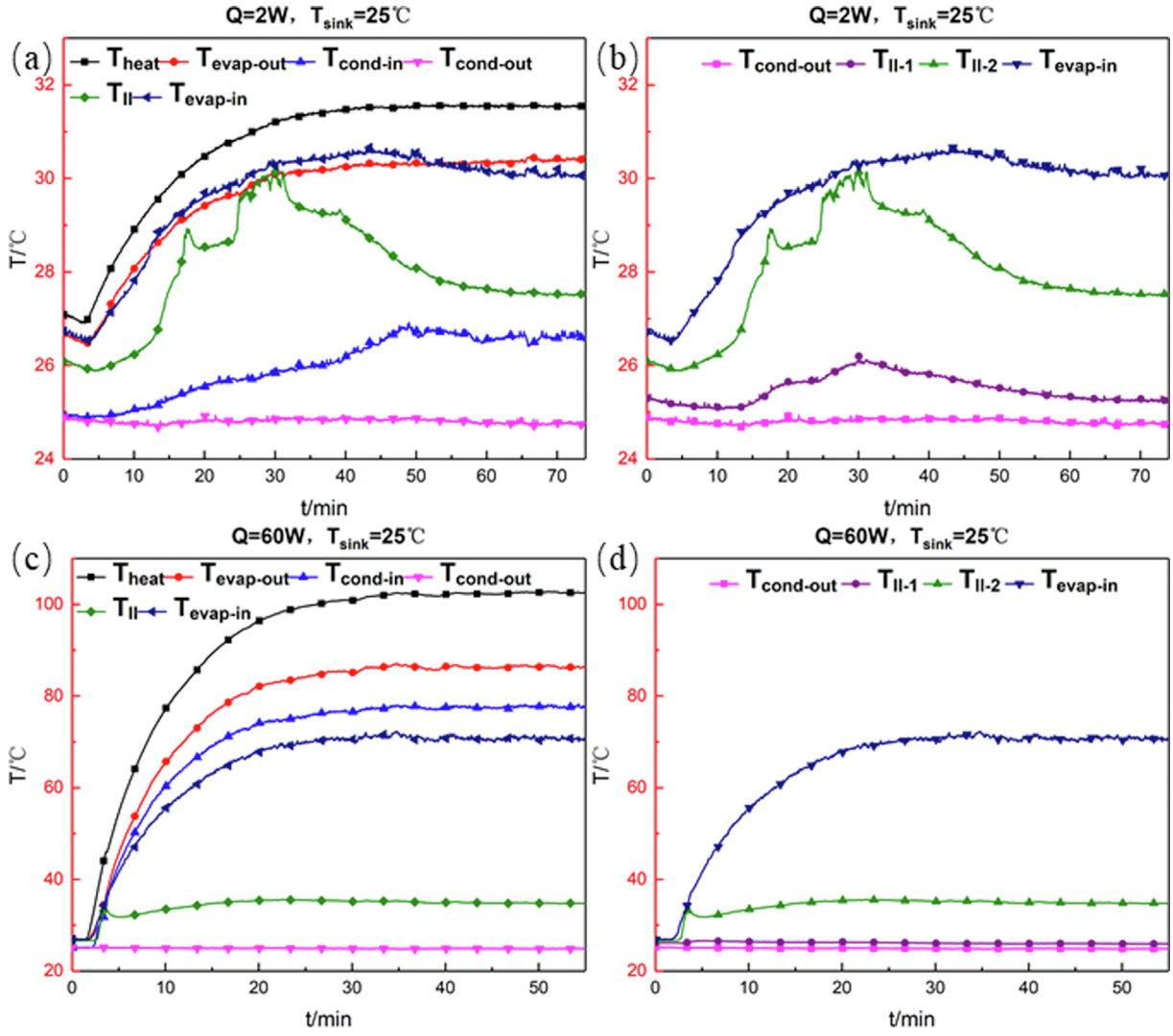

Fig. 9. The temperature of the mLHP at the sink temperature of 25 °C.

the operation state of mLHP. At low heat load, the circulation speed and mass circulation rate of the working fluid are extremely low. Conversely, most of the condenser is filled with the liquid form of the working fluid, and the efficiency of the condenser is low. The returning supercooled fluid does not offset the heat leak of the compensation chamber. In contrast, there is a liquid of the working fluid in the vapor grooves, and the evaporation is increasingly difficult when the heated surface is covered with a liquid film. With increases in the heat load, the redistribution of the working fluid in the vapor grooves is faster, and the mass circulation rate of the working fluid increases. Thus, the thermal resistance of LHP decreases. The R_{evap} of present mLHP remains at approximately 0.27 °C/W when the heat load exceeds 40 W. The thermal resistance increases with increases in the heat load after the constant thermal resistance stage due to the hyperthermia, more significant heat leak and failures of the wick. It can be assumed that there will be a higher temperature difference between the evaporator and the compensation chamber at the heat load of 60 W. The constraints of the mLHP operation performance correspond to high pressure and temperature difference.

With respect to the sink temperature, it does not significantly affect the thermal resistance. It is observed that the R_{evap} remains the same at a different sink temperature with the 60 W heat load. Additionally, R_{LHP} and R_{sys} fluctuate although it remains at the same level as 0.8 °C/W and 1.3 °C/W.

4. Conclusion

In the present study, a miniature LHP with an eccentric evaporator of 4.5-mm thickness was proposed. The mLHP included tests under different heat loads ranging from 2 W to 60 W and different sink temperatures ranging from 0 °C to 35 °C to investigate startup behavior and operation characteristics. A few conclusions are obtained from the results as follows:

(1) The mLHP with an eccentric evaporator can successfully start up at a heat load of 2 W in the horizontal orientation with different sink temperatures ranging from 0 °C to 25 °C. The minimum heat load corresponded to 5 W at the sink temperature of 35 °C. The mLHP transported the maximum heat load of 60 W at different sink temperatures from 0 °C to 35 °C with a larger heat load range for stable operation.
(2) The impact of different sink temperature on mLHP performance was analyzed by thermal network method and verified in the experiment. It could be inferred the operation temperature of mLHP will increase with increases in the temperature of the sink due to the deterioration of the thermal environment deterioration in the compensation chamber.
(3) A minimum thermal resistance of the evaporator R_{evap} equal to 0.27 °C/W was achieved at a maximum heat load of 60 W. The value of R_{LHP} and R_{sys} were 0.8 °C/W and 1.3 °C/W, respectively.

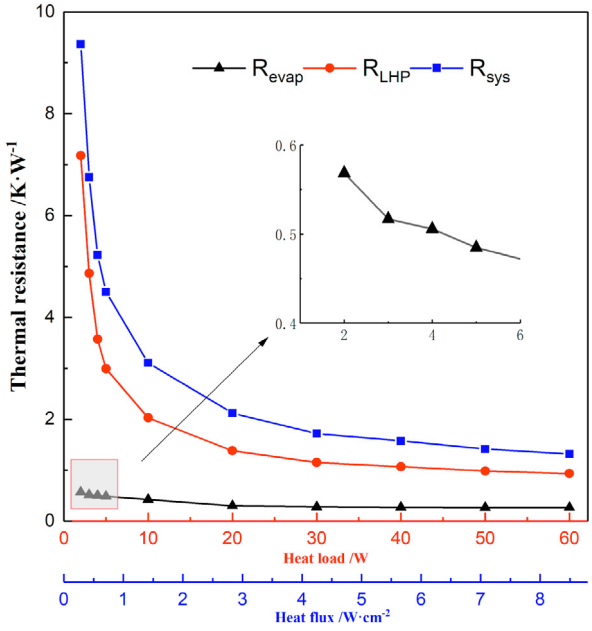

(a) Thermal resistance at different heat loads, T_{sink}=10 °C

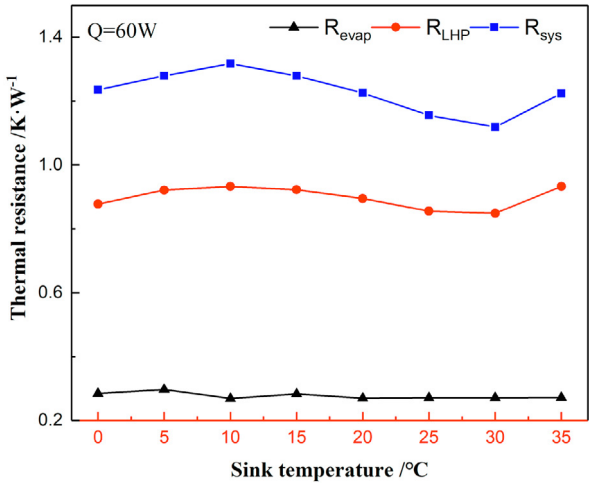

(b) Thermal resistance at different sink temperatures, Q=60 W

Fig. 10. Analysis of thermal resistance.

Additionally, the sink temperature difference had not significantly affect on all thermal resistance of the mLHP.

(4) The proposed mLHP with eccentric structure exhibited a good response to low heat load and operation behavior. The study proposes a novel and promising way to improve the performance of LHP as a thermal control method for electronics.

Acknowledgment

The study is supported by the National Natural Science Foundation of China [Grant Nos. 51776079 & 51376004]; and the National Key Research and Development Program of China [Grant Nos.2017YFB0603501-3].

Appendix A. Supplementary material

Supplementary data to this article can be found online at https://doi.org/10.1016/j.applthermaleng.2019.113982.

References

[1] V.G. Pastukhov, Y.F. Maidanik, C.V. Vershinin, M.A. Korukov, Miniature loop heat pipes for electronics cooling, Appl. Therm. Eng. 23 (2003) 1125–1135.
[2] Y.F. Maydanik, S.V. Vershinin, V.G. Pastukhov, S. Fried, Loop heat pipes for cooling systems of servers, IEEE Trans. Compon. Packag. Technol. 33 (2010) 416–423.
[3] C.C. Yeh, B.H. Liu, Y.M. Chen, A study of loop heat pipe with biporous wicks, Heat Mass Transf. 44 (2008) 1537–1547.
[4] B.B. Chen, W. Liu, Z.C. Liu, H. Li, J.G. Yang, Experimental investigation of loop heat pipe with flat evaporator using biporous wick, Appl. Therm. Eng. 42 (2012) 34–40.
[5] S. He, J. Zhao, Z.C. Liu, et al., Experimental investigation of loop heat pipe with a large squared evaporator for cooling electronics, Appl. Therm. Eng. 144 (2018) 383–391.
[6] D. Gai, Z. Liu, W. Liu, J. Yang, Operational characteristics of miniature loop heat pipe with flat evaporator, Heat Mass Transf. 46 (2009) 267–275.
[7] Z. Liu, D. Gai, H. Li, W. Liu, J. Yang, M. Liu, Investigation of impact of different working fluids on the operational characteristics of miniature LHP with flat evaporator, Appl. Therm. Eng. 31 (2011) 3387–3392.
[8] Y.F. Maydanik, M.A. Chernysheva, V.G. Pastukhov, Review: loop heat pipes with flat evaporators, Appl. Therm. Eng. 67 (2014) 294–307.
[9] K. Fukushima, H. Nagano, New evaporator structure for micro loop heat pipes, Int. J. Heat Mass Transf. 106 (2017) 1327–1334.
[10] A.A. Adoni, A. Ambirajan, V.S. Jasvanth, D. Kumar, P. Dutta, Theoretical and experimental studies on an ammonia-based loop heat pipe with a flat evaporator, IEEE Trans. Compon. Packag. Technol. 33 (2010) 478–487.
[11] G. Zhou, J. Li, L. Lv, An ultra-thin miniature loop heat pipe cooler for mobile electronics, Appl. Therm. Eng. 109 (2016) 514–523.
[12] X. Zhang, J. Huo, S. Wang, Experimental investigation on temperature oscillation in a miniature loop heat pipe with flat evaporator, Exp. Therm. Fluid Sci. 37 (2012) 29–36.
[13] S. Wang, J. Huo, X. Zhang, Z. Lin, Experimental study on operating parameters of miniature loop heat pipe with flat evaporator, Appl. Therm. Eng. 40 (2012) 318–325.
[14] < Micro loop heat pipe for mobile electronics applications.pdf > .
[15] R. Singh, A. Akbarzadeh, M. Mochizuki, Operational characteristics of a miniature loop heat pipe with flat evaporator, Int. J. Therm. Sci. 47 (2008) 1504–1515.
[16] R. Singh, A. Akbarzadeh, M. Mochizuki, Thermal potential of flat evaporator miniature loop heat pipes for notebook cooling, IEEE Trans. Compon. Packag. Technol. 33 (2010) 32–45.
[17] H. Tang, Y. Tang, W. Yuan, R. Peng, L. Lu, Z. Wan, Fabrication and capillary characterization of axially micro-grooved wicks for aluminium flat-plate heat pipes, Appl. Therm. Eng. 129 (2018) 907–915.
[18] J. Esarte, J.M. Blanco, A. Bernardini, J.T. San-José, Optimizing the design of a two-phase cooling system loop heat pipe: Wick manufacturing with the 3D selective laser melting printing technique and prototype testing, Appl. Therm. Eng. 111 (2017) 407–419.
[19] Y. Maydanik, S. Vershinin, M. Chernysheva, S. Yushakova, Investigation of a compact copper–water loop heap pipe with a flat evaporator, Appl. Therm. Eng. 31 (2011) 3533–3541.
[20] Y.F. Maydanik, V.G. Pastukhov, M.A. Chernysheva, Development and investigation of a miniature copper-acetone loop heat pipe with a flat evaporator, J. Electron. Cooling Therm. Control 05 (2015) 77–88.
[21] W. Joung, T. Yu, J. Lee, Experimental study on the loop heat pipe with a planar bifacial wick structure, Int. J. Heat Mass Transf. 51 (2008) 1573–1581.
[22] B.J. Huang, H.H. Huang, T.L. Liang, System dynamics model and startup behavior of loop heat pipe, Appl. Therm. Eng. 29 (2009) 2999–3005.
[23] D. Wang, Z. Liu, J. Shen, C. Jiang, B. Chen, J. Yang, Z. Tu, W. Liu, Experimental study of the loop heat pipe with a flat disk-shaped evaporator, Exp. Therm Fluid Sci. 57 (2014) 157–164.
[24] D. Wang, Z. Liu, S. He, J. Yang, W. Liu, Operational characteristics of a loop heat pipe with a flat evaporator and two primary biporous wicks, Int. J. Heat Mass Transf. 89 (2015) 33–41.
[25] H. Song, L. Zhi-chun, Z. Jing, J. Chi, Y. Jin-guo, L. Wei, Experimental study of an ammonia loop heat pipe with a flat plate evaporator, Int. J. Heat Mass Transf. 102 (2016) 1050–1055.